PHYSICAL REVIEW B **94**, 081401(R) (2016)

Free-standing electronic character of monolayer MoS_2 in van der Waals epitaxy

HoKwon Kim (김호권),[1,2,*] Dumitru Dumcenco,[1,2] Mathieu Frégnaux,[3,4,†] Anass Benayad,[3,5] Ming-Wei Chen,[1,2] Yen-Cheng Kung,[1,2] Andras Kis,[1,2] and Olivier Renault[3,4]

[1]*Electrical Engineering Institute, École Polytechnique Fédérale de Lausanne (EPFL), CH-1015 Lausanne, Switzerland*

[2]*Institute of Materials Science and Engineering, École Polytechnique Fédérale de Lausanne (EPFL), CH-1015 Lausanne, Switzerland*

[3]*Université Grenoble Alpes, F-38000 Grenoble, France*

[4]*CEA, LETI, MINATEC Campus, F-38054 Grenoble, France*

[5]*Department of Nanomaterials, CEA, LITEN, MINATEC, F-38054 Grenoble, France*

(Received 24 March 2016; revised manuscript received 8 June 2016; published 1 August 2016)

We have evaluated as-grown MoS_2 crystals, epitaxially grown on a monocrystalline sapphire by chemical vapor deposition (CVD), with direct electronic band-structure measurements by energy-filtered k-space photoelectron emission microscopy performed with a conventional laboratory vacuum ultraviolet He I light source under *off*-normal illumination. The valence states of the epitaxial MoS_2 were mapped in momentum space down to 7 eV below the Fermi level. Despite the high nucleation density within the imaged area, the CVD MoS_2 possesses an electronic structure similar to the free-standing monolayer MoS_2 single crystal, and it exhibits hole effective masses of $2.41 \pm 0.05\, m_0$, and $0.81 \pm 0.05\, m_0$, respectively, at Γ and K high-symmetry points that are consistent with the van der Waals epitaxial growth mechanism. This demonstrates the excellent ability of the MoS_2 CVD on sapphire to yield a highly aligned growth of well-stitched grains through epitaxial registry with a strongly preferred crystallographic orientation.

DOI: 10.1103/PhysRevB.94.081401

Monolayer MoS_2 has gained significant attention recently as one of the most promising semiconductor materials for development of future generation electronic devices beyond the conventional silicon-based electronics. A large number of studies have been performed on proof-of-principle devices which exploit the unique two-dimensional (2D) properties of the direct band-gap three-atom-thick semiconductor [1–3]. In the aim of scaling up the fabrication process of MoS_2-based devices, large-area chemical vapor deposition (CVD) of MoS_2 layers has been demonstrated on centimeter scale substrates, such as SiO_2 and sapphire. Especially, monolayer MoS_2 growth on c-sapphire has successfully demonstrated to produce well-aligned CVD MoS_2 monolayer flakes where more than 90% of the single-crystalline monolayers exhibit preferred crystallographic alignment [4]. This allows for the van der Waals epitaxy of large-area monolayer domains with seamlessly stitched monolayer MoS_2 grains.

The monolayer MoS_2 is known to feature a unique electronic band structure, such as tunable indirect-direct band-gap transition by mechanical strain and spin-orbit-induced splitting at K and K' points that enables spin-valley polarization [5–7]. For further use of epitaxial MoS_2, it is crucial to carefully examine the electronic structure of the epitaxial domains and compare it to the pristine free-standing monolayer MoS_2 since MoS_2 grown by CVD can exhibit a biaxial in-plane strain due to lattice expansion coefficient mismatch, impurities, and nonstoichiometric chemical states due to crystal defects, such as vacancies and grain boundaries. The charge transport, photoluminescence (PL), and Raman spectroscopy measurements have already indicated that the CVD MoS_2 monolayers exhibit similar electronic qualities as exfoliated MoS_2 monolayers obtained by the adhesive tape method [4]. Furthermore, the direct imaging of the electronic band structure of as-grown epitaxial MoS_2 is realized here. The three-dimensional electronic structure images can provide valuable information regarding direct-to-indirect band-gap transition, presence of multiple polymorphs, and the anisotropic effect of mechanical strain. Jin *et al.* [8] have observed an upper valence-band (UVB) compression of ∼50% by synchrotron radiation k-resolved photoelectron emission microscopy (kPEEM) in CVD MoS_2 grown on SiO_2/Si by transferring the as-grown film onto highly doped Si using a polymer support. They attributed this band distortion to the various effects, such as defects, doping, strain, impurities, and interaction with the substrate which may all be affected by the transfer process. The lack of the direct band-structure imaging on as-grown epitaxial MoS_2 was largely due to the difficulty of growing a large single crystal of MoS_2 bigger than tens of microns—a size suitable enough for the reciprocal space imaging and insulating substrate that results in charging of the sample under the incident x-ray or UV illumination.

Here, we performed PEEM on an as-grown CVD monolayer MoS_2 on a dielectric substrate using a laboratory UV source in order to directly probe its electronic structure without any transfer process. This is achieved, first, by implementing energy-filtered momentum microscopy kPEEM, which is a facile way to obtain access to band-structure mapping of well-defined features in k space thanks to the parallel angular imaging over a spatially resolved area as small as 5 μm^2 [9,10]. For example, it was applied successfully for unravelling a complex stacking in the form of commensurate rotations of few-layer graphene in SiC(000-1), either using conventional bright-field PEEM [9] (Ref. [6]) or more subtle dark-field PEEM [11]. The reliability and efficiency (no sample rotation as in conventional angle-resolved photoemission spectroscopy, together with analysis of the full reciprocal space in one

*hknano@gmail.com

†Present address: Institut Lavoisier de Versailles (ILV), UMR CNRS 8180, Université de Versailles Saint-Quentin-en-Yvelines, F-78035 Versailles, France.

acquisition run) of this fast analytical method is of high interest for evaluating the electronic properties of 2D materials and related processes. Second, we applied a careful sample preparation method by depositing a gold (Au) electrode across the substrate over continuous fully stitched single-crystalline MoS_2 grains. The Au contact allowed us to perform *k*PEEM of a CVD-grown MoS_2 monolayer from the domain of ~20-μm lateral size below the Fermi level without a significant charging effect as the film is electrically contacted to the sample holder. This Rapid Communication demonstrates that reliable *k*PEEM measurements of the band structure of clean 2D materials on insulating substrates can be performed using a conventional laboratory UV source, thereby providing direct measurements of important electronic properties, such as charge-carrier effective mass, upper valence-band characteristics, and MoS_2 band-structure distortion likely induced by the substrate.

The CVD MoS_2 on a single-crystal c-sapphire substrate (1×1 cm^2) was produced by the procedure previously reported by Dumcenco *et al.* [4]. The growth conditions were selected specifically to produce a continuous monolayer film with an average grain size of 5 μm. The MoS_2 coverage and crystal alignment were verified by reflection high-energy electron diffraction (RHEED) as shown in Fig. S1 (see Supplemental Material [12]). The Raman and photoluminescence spectroscopy mappings [Fig. S2 (see Supplemental Material [12])] in the lateral length scale of *k*PEEM measurements were performed to study the thickness uniformity and optical quality of the film. The details of the RHEED, Raman, and PL spectroscopies can be found in the Supplemental Material [12].

On the as-grown CVD film, the Au stripes [Fig. 1(a)] were evaporated by an electron beam through a patterned shadow mask with a final thickness of 84 nm. This allowed the MoS_2 overlayer on the substrate to be electrically contacted to the stainless-steel PEEM sample holder, which is held at a constant near-ground potential. This is similar to the method employed by Locatelli *et al.* [13] in order to obtain band-structure imaging of exfoliated graphene on SiO_2 without detrimental charging effects. The Au patterns could also serve as markers which enabled a facile spatial identification of the area of interest by optical microscopy, PEEM, and x-ray photoemission spectroscopy (XPS).

The *k*PEEM analysis was performed with a *NanoESCA* MkI spectromicroscope (ScientaOmicron) [14–16] in ultra-high-vacuum conditions and at ambient temperature. An He I cold cathode lamp ($h\nu = 21.2$ eV) was employed as a laboratory vacuum-ultra-violet excitation source impinging the sample in an *off*-normal direction, namely, at an angle of 65° with respect to the sample normal. So-called *k*PEEM, momentum-resolved images were acquired over the full surface first Brillouin zone (± 1.8 Å^{-1}). The high-energy resolution momentum images were recorded at a spectrometer pass energy of 25 eV and a 1-mm diameter entrance slit of the imaging spectrometer (equivalent to an overall energy resolution of ~0.2eV) and with low-noise event-counting detection allowing enhanced sensitivity for precise upper valence-band analysis. It is important to note that this energy resolution is the same as typical momentum microscopy measurements performed with synchrotron radiation and reported to date [8]. Compared to the experimental conditions of the work of Jin *et al.* [8], the off-normal illumination used here enhances the intensity at the Γ point through favorable transition probability from the out-of-plane Mo $4d_z^2$ orbitals, which is crucial for a direct analysis of the energy dispersion curves [17]. A careful calibration of the *k*-space scale was performed by measuring with identical PEEM settings as applied for the MoS_2 sample the known reciprocal lattice distances of a freshly prepared Cu(111) single-crystal surface. After the flat field and dark-noise subtraction, the Poisson noise originating from the image counting mode was reduced by postprocessing with the IMAGEJ PUREDENOISE plug-in [18,19]. A second derivative of each image series was taken in order to enhance the contrast of the band dispersion maps.

We have also performed micron-scale XPS measurements thanks to a scanning x-ray microprobe spectrometer (ULVAC-PHI 5000 Versa Probe II) equipped with a laboratory Al *Kα* source ($h\nu = 1486.6$ eV). The x-ray spot size was 18 μm, and the overall energy resolution was 0.6 eV for high-energy resolution core-level acquisition. A dual-beam charge neutralizer was employed jointly a low-energy Ar ion, and an electron gun was used while performing XPS with the Versa Probe II instrument as the sample was not grounded in this case due to the setup geometry. The spectra offset was adjusted according to the C 1*s* peak originating from the surface adventitious carbon contamination with a reference binding energy position at 284.8 eV.

Figure 1(a) shows the optical microscope image of monolayer MoS_2 grown on sapphire. Before the PEEM investigation, the overall uniformity and coverage of the MoS_2 layer was verified by optical microscopy. The CVD growth could reproducibly yield large single-crystal monolayer grains on the order of 1 μm or bigger where most of them are merged to form seamlessly stitched single-crystal MoS_2 without grain boundaries due to the preferential alignment of the MoS_2 grains on the single-crystal substrate. The crystal alignment, thickness uniformity, and optical quality of our sample was further verified by RHEED (see the Supplemental Material (Fig. S1) [12]), Raman spectroscopic mapping (Fig. S2b) and photoluminescence peak position mapping (Fig. S2e). Additionally, the spatially resolved XPS in the Mo 3*d* binding energy region [Fig. 1(b)] demonstrates a Mo binding energy shift in agreement with that of an ideal MoS_2 crystal. The main peaks related to the pristine MoS_2; $Mo^{4+}3d_{5/2}$ and $3d_{3/2}$ doublet peaks (located at 229.1 and 232.2 eV) and the S 2*s* peak (located at 226.3 eV) are prominent in Fig. 1(b) [20–22]. The small peak at ~235.5 eV is likely arising from the Mo^{6+} $3d_{3/2}$ chemical state as a result of slight oxidation of the sample at a small fraction of grain boundaries or other crystalline defects within the sample [20].

The *k*-space-area-integrated spectrum of the upper valence-band region in Fig. 1(c) reveals that that the Fermi edge is about 1.6 eV above the valence-band maximum. This *n* doping of the film is expected due to the commonly reported prevalence of sulfur vacancies in MoS_2 [23,24].

The *k*PEEM images in the UVB region were acquired from a uniform area of the sample with a typical field aperture diameter of ~30 μm; these are shown in Fig. 2 for different binding energies below the valence-band maximum level E_{VBM}. It can be clearly seen that distinct band structures can be observed at 0–6 eV below E_{VBM} with hexagonal

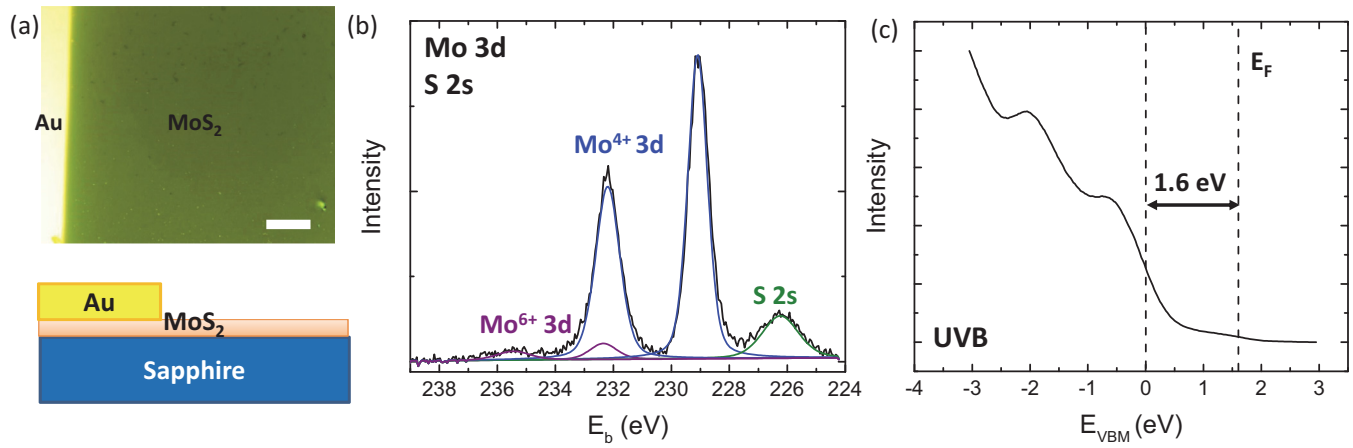

FIG. 1. (a) (Top) Optical microscopy image of MoS_2/sapphire with a Au contact. Scale bar: 25 μm. (Bottom) Schematic of a Au contact on MoS_2/c sapphire. (b) Background subtracted core-level XPS spectra of the Mo 3*d*, S 2*s* peak regions from a uniform monolayer area. (c) First Brillouin-zone angle-integrated valence-band spectrum from *k*PEEM measurements. The dotted lines represent the positions of the Fermi level (E_F) edge and upper valence-band edge.

symmetry, clearly demonstrating the preferential alignment of single-crystalline grains of the epitaxial MoS_2. The cut along the high-symmetry directions ($MK\Gamma$) of the three-dimensional stack of the *k*-space images is shown in Fig. 3. The dispersion relationships along these high-symmetry directions are important in determining the optoelectronic properties of the film. The band-structure predictions based on the density-functional-theory (DFT) calculations performed by Jin *et al.* [17] have also been superimposed onto the color map. Unlike the previous report on the uppermost valence band at the Γ point obtained with the synchrotron radiation excitation energy of 42 eV (i.e., at the Cooper minimum of the S 3*p* orbitals) [8], the intensity of the photoelectron is higher thanks to the increased cross section at the He I discharge energy of 21.2 eV for the Mo $4d_z^2$ related bands and enhanced transition probability under more grazing photon excitation. Notably, the *K* and Γ points are almost at the same energy level within the margin of error of $\pm$0.1eV partly due to the broadening at the *K* point induced by the enhanced spin-orbit splitting in MoS_2 that remains unresolved here. Also, we cannot exclude a broadening at the Γ point due to contributions from the S $3p_z$ orbitals, the cross section of which at 21.2-eV excitation energy is about 25% that of the Mo $4d_z^2$ orbitals. We note that an increasing band broadening in monolayer exfoliated MoS_2 was reported recently by Jin *et al.* [17], the origin of which is still unclear. Nevertheless, this result is consistent with the characteristic of unstrained monolayer MoS_2. Thus,

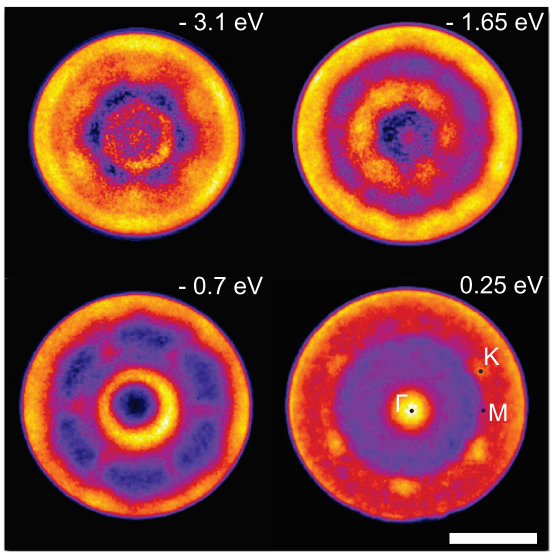

FIG. 2. *k*PEEM images of as-grown MoS_2/sapphire acquired at different binding energies. The numbers at the top-right corner denote the E_{VBM} values for each image. Note that the image intensities have been normalized with a background removal filter in order to enhance the contrast for each image. The scale bar is 1 $Å^{-1}$. A set of high-symmetry points (Γ, *M*, and *K*) is indicated by black dots. $h\nu$ = 21.2 eV; analyzer energy resolution of 0.2 eV; *k*-space resolution of $\sim$0.05 $Å^{-1}$ acquisition time per image = 80 s.

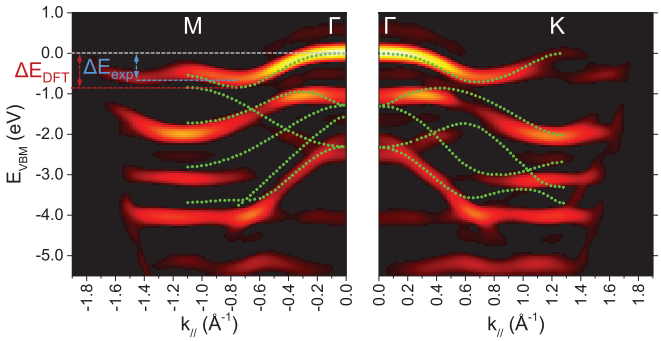

FIG. 3. Electronic band structure of the monolayer MoS_2 on c sapphire along high-symmetry points *M*, Γ, and *K*. Theoretical band structure predicted by DFT calculations for a free-standing monolayer MoS_2 from Jin *et al.* [17] has been superimposed as green dots. The dashed horizontal lines and double-headed arrows indicate the widths of the uppermost valence band of the DFT calculations (ΔE_{DFT}) and the actual experiment (ΔE_{exp}). The signal-to-noise ratio was enhanced by taking the second derivative of the *k*PEEM intensity and a steerable filter [27] for each image.

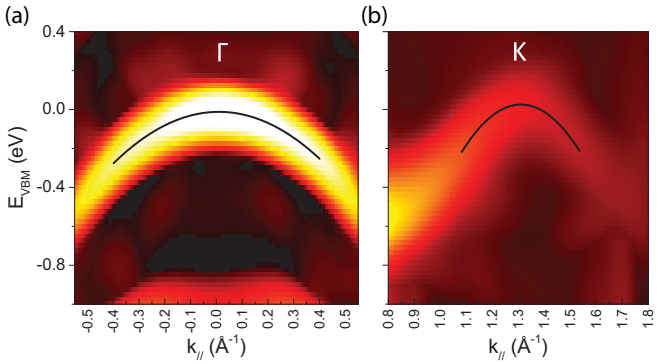

FIG. 4. High-resolution electronic band-structure monolayer MoS_2 (a) near the Γ point and (b) near the K point. The black solid lines near the local band maxima represent a parabolic fitting of the dispersion relationship for the effective mass calculation. The signal-to-noise ratio was enhanced by taking the second derivative of the kPEEM intensity and a steerable filter [27] for each image.

the electronic band structure appears to be similar to that of free-standing single-crystalline monolayer MoS_2. This is expected for the van der Waals epitaxial growth mechanism where the substrate does not significantly influence the electronic structure through orbital hybridization or by inducing significant mechanical strain in the lattice structure during the growth or cool-down process. We rule out the presence of a significant in-plane strain in the layer since the measured ΓK distance $1.34\,\text{Å}^{-1}$ is very close within the range of error to the standard value of $1.326\,\text{Å}^{-1}$ for the surface of the first Brillouin zone of bulk MoS_2. This is consistent with the expected strain value of ∼0.1% considering the van der Waals epitaxial relationship with the substrate and the small thermal lattice expansion coefficient mismatch [4]. This almost negligible in-plane strain is in contrast with what was observed recently on both suspended and supported exfoliated MoS_2 which reported a surface in-plane lattice expansion of about 3.6% compared to bulk MoS_2 [17].

One can estimate the hole effective mass at each high-symmetry point of the first Brillouin zone by analyzing the curvature of the UVB. Within the free-electron approximation, the two-dimensional shape of the UVB is given by the equation $E = \hbar^2 k^2/2m^*$, where $\hbar$ is the reduced Planck constant and m^* is the effective mass of the charge carrier. From the electronic band structure obtained with a 25-eV pass energy setting, we performed a series of Gaussian fittings on the energy distribution curves (EDCs) (see the Supplemental Material Fig. S3 [12]) to trace dispersion relationships near the high-symmetry points in Fig. 4. The parabolic curve fitting of the band dispersion yielded the effective mass of $2.41 \pm 0.05\,m_0$ at Γ and $0.81 \pm 0.05\,m_0$ at K where m_0 is the electron rest mass. The effective mass at Γ matches closely with the theoretical values reported in literature [8]. However, the effective mass at the K point appears to be significantly higher than the expected values from the other experiments or DFT calculations which range from 0.43 to $0.64m_0$ [8]. This is probably due to the increase in uncertainty in the effective mass calculations where spin-orbit splitting leads to a broadening of the band, although the energy resolution was not high enough to resolve the splitting as also reported by Jin *et al.* [17]. As a result, only a single-peak Gaussian fitting was used to analyze the EDCs at the K point. The electronic states at the K point derive from in-plane Mo $d(x^2 - y^2)/d_{xy}$ orbitals and therefore, only a significant in-plane strain is expected to affect the derived value of the effective mass. This is not the case here because no significant strain was observed and the c-sapphire substrate does not have a significant density of states near the VBM of MoS_2 unlike the MoS_2/graphene system where charge-transfer-induced strain for certain twist angles can change the positions of band maxima [25]. Moreover, the overlap between the electronic states of misaligned grains, which comprise less than 10% of the grains, might have contributed to the broadening of the dispersion relationship which increased the uncertainty in the extracted values of the effective mass. In sum, we believe that an increased uncertainty due to band broadening at K is the main reason explaining the derived effective mass value. Further work is underway in order to clearly resolve the band splitting arising from the spin-orbit coupling using improved energy resolution conditions and detection efficiency.

We have also observed a band compression effect in the band structure of the MoS_2 grains where the energy width of the uppermost branch of the valence band (ΔE_{exp} in Fig. 3) is compressed by ∼82% with respect to the free-standing MoS_2 sample of Jin *et al.* [8] matching very well with their DFT calculations (ΔE_{DFT} in Fig. 3). This value of the "compression factor" is much smaller than that of the transferred CVD monolayer MoS_2 flake on the Si(111) substrate [8] and similar to the one reported for supported MoS_2 on SiO_2 produced by the adhesive tape exfoliation method. This valence-band compression can be attributed to the presence of the sapphire substrate since this has not been observed for the free-standing MoS_2. The substrate likely induced a weak interaction with the bottom layer of S possibly leading to substrate-induced corrugations, Mo-S bond length variations, or changes in the dielectric environment as similarly suggested for MoS_2 on Si (111) [8,25]. The detailed modeling of the van der Waals interaction between MoS_2 and c sapphire and the resulting interfacial state is out of the scope of the current Rapid Communication as the realistic predictions of the band structure require computationally challenging techniques [26]. Nevertheless, the influence of the substrate on the band structure is to be investigated in the future by considering other CVD monolayer MoS_2/substrate systems and further theoretical calculations.

To summarize, the electronic structure of a large-area as-grown CVD MoS_2 monolayer was directly measured by energy-filtered momentum microscopy kPEEM using a conventional He I excitation source under *off*-normal illumination. The full k-space imaging of the valence-band structure verifies the exceptional crystal quality of the van der Waals epitaxy of MoS_2 on a c-sapphire substrate and demonstrates a free-standing character of the single-crystal MoS_2 obtained. We report a negligible in-plane relaxation and effective hole mass of $2.41 \pm 0.05\,m_0$ and $0.81 \pm 0.05\,m_0$, respectively, at Γ and K high-symmetry points. The upper valence band appeared to be compressed by 82% compared to that of free-standing MoS_2 suggesting the band distorting effect of the substrate. This Rapid Communication has a strong implication on the

band-structure engineering of MoS_2 monolayers for digital and optoelectronic applications.

H.K. acknowledges the French CEA Basic Technological Research program (RTB) for postdoctoral funding and M. Audiffred for helpful conversations. The main experimental work was performed at the Nanocharacterization Platform (PFNC) of MINATEC Research Centre, CEA-Grenoble. This work was financially supported by the Graphene Flagship (Grant Agreement No. 604391), Swiss SNF Sinergia Grant No. 147607, and Marie Curie ITN network "MoWSeS" (Grant No. 317451).

[1] B. Radisavljevic, A. Radenovic, J. Brivio, V. Giacometti, and A. Kis, Nat. Nanotechnol. **6**, 147 (2011).
[2] R. Kappera, D. Voiry, S. E. Yalcin, B. Branch, G. Gupta, A. D. Mohite, and M. Chhowalla, Nat. Mater. **13**, 1128 (2014).
[3] D. Krasnozhon, D. Lembke, C. Nyffeler, Y. Leblebici, and A. Kis, Nano Lett. **14**, 5905 (2014).
[4] D. Dumcenco, D. Ovchinnikov, K. Marinov, P. Lazić, M. Gibertini, N. Marzari, O. L. Sanchez, Y.-C. Kung, D. Krasnozhon, M.-W. Chen, S. Bertolazzi, P. Gillet, A. Fontcuberta i Morral, A. Radenovic, and A. Kis, ACS Nano **9**, 4611 (2015).
[5] T. Cao, G. Wang, W. Han, H. Ye, C. Zhu, J. Shi, Q. Niu, P. Tan, E. Wang, B. Liu, and J. Feng, Nat. Commun. **3**, 887 (2012).
[6] K. F. Mak, K. He, J. Shan, and T. F. Heinz, Nat. Nanotechnol. **7**, 494 (2012).
[7] T. Jiang, H. Liu, D. Huang, S. Zhang, Y. Li, X. Gong, Y.-R. Shen, W.-T. Liu, and S. Wu, Nat. Nanotechnol. **9**, 825 (2014).
[8] W. Jin, P.-C. Yeh, N. Zaki, D. Zhang, J. T. Sadowski, A. Al-Mahboob, A. M. van der Zande, D. A. Chenet, J. I. Dadap, I. P. Herman, P. Sutter, J. Hone, and R. M. Osgood, Phys. Rev. Lett. **111**, 106801 (2013).
[9] C. Mathieu, N. Barrett, J. Rault, Y. Y. Mi, B. Zhang, W. A. de Heer, C. Berger, E. H. Conrad, and O. Renault, Phys. Rev. B **83**, 235436 (2011).
[10] C. Mathieu, O. Renault, H. Rotella, N. Barrett, and A. Chabli, AIP Conf. Proc. **1395**, 95 (2011).
[11] N. Barrett, E. Conrad, K. Winkler, and B. Krömker, Rev. Sci. Instrum. **83**, 083706 (2012).
[12] See Supplemental Material at http://link.aps.org/supplemental/10.1103/PhysRevB.94.081401 for the experimental methods and supplemental figures for RHEED, Raman, and PL spectroscopies, and details of the EDC analysis.
[13] A. Locatelli, K. R. Knox, D. Cvetko, T. O. Menteş, M. A. Niño, S. Wang, M. B. Yilmaz, P. Kim, R. M. Osgood, and A. Morgante, ACS Nano **4**, 4879 (2010).
[14] M. Escher, N. Weber, M. Merkel, C. Ziethen, P. Bernhard, G. Schönhense, S. Schmidt, F. Forster, F. Reinert, B. Krömker, and D. Funnemann, J. Phys.: Condens. Matter **17**, S1329 (2005).
[15] M. Escher, K. Winkler, O. Renault, and N. Barrett, J. Electron Spectrosc. Relat. Phenom. **178–179**, 303 (2010).
[16] B. Krömker, M. Escher, D. Funnemann, D. Hartung, H. Engelhard, and J. Kirschner, Rev. Sci. Instrum. **79**, 053702 (2008).
[17] W. Jin, P.-C. Yeh, N. Zaki, D. Zhang, J. T. Liou, J. T. Sadowski, A. Barinov, M. Yablonskikh, J. I. Dadap, P. Sutter, I. P. Herman, and R. M. Osgood, Phys. Rev. B **91**, 121409 (2015).
[18] F. Luisier and T. Blu, IEEE Trans. Image Process. **17**, 482 (2008).
[19] PUREDENOISE, http://bigwww.epfl.ch/algorithms/denoise, 2015.
[20] T. L. Barr, J. Chem. Phys. **82**, 1801 (1978).
[21] T. Weber, J. C. Muijsers, J. H. M. C. van Wolput, C. P. J. Verhagen, and J. W. Niemantsverdriet, J. Chem. Phys. **100**, 14144 (1996).
[22] E. Buzaneva, T. Vdovenkova, A. Gorchinsky, A. Senkevich, V. Nemoshkalenko, A. Klein, and Y. Tomm, J. Electron Spectrosc. Relat. Phenom. **68**, 763 (1994).
[23] J. Suh, T.-E. Park, D.-Y. Lin, D. Fu, J. Park, H. J. Jung, Y. Chen, C. Ko, C. Jang, Y. Sun, R. Sinclair, J. Chang, S. Tongay, and J. Wu, Nano Lett. **14**, 6976 (2014).
[24] R. Addou, S. McDonnell, D. Barrera, Z. Guo, A. Azcatl, J. Wang, H. Zhu, C. L. Hinkle, M. Quevedo-Lopez, H. N. Alshareef, L. Colombo, J. W. P. Hsu, and R. M. Wallace, ACS Nano **9**, 9124 (2015).
[25] W. Jin, P.-C. Yeh, N. Zaki, D. Chenet, G. Arefe, Y. Hao, A. Sala, T. O. Mentes, J. I. Dadap, A. Locatelli, J. Hone, and R. M. Osgood, Phys. Rev. B **92**, 201409 (2015).
[26] A. K. Singh, R. G. Hennig, A. V. Davydov, and F. Tavazza, Appl. Phys. Lett. **107**, 053106 (2015).
[27] M. Jacob and M. Unser, IEEE Trans. Pattern Anal. Mach. Intell. **26**, 1007 (2004).